Imaging and detection of early stage dental caries with an all-optical photoacoustic microscope

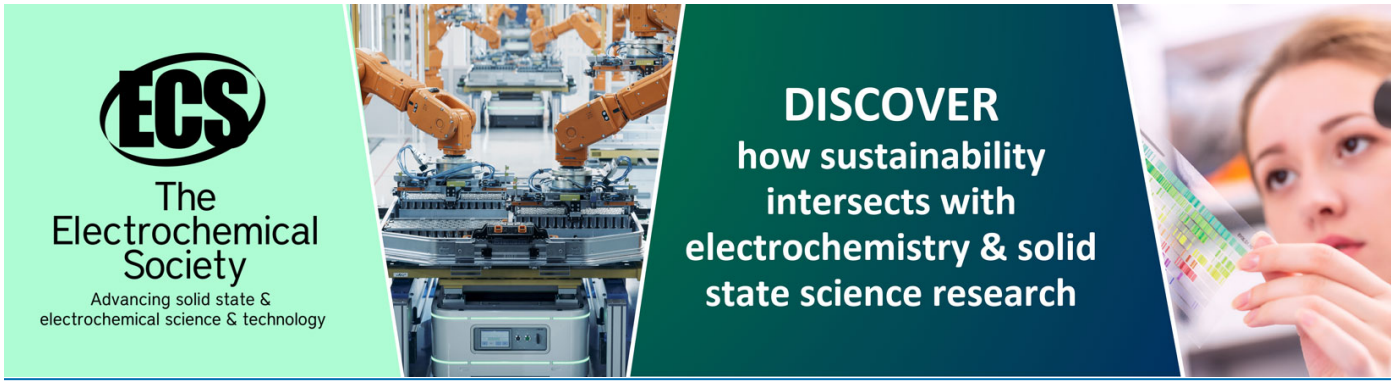

Journal of Physics: Conference Series **581** (2015) 012002 doi:10.1088/1742-6596/581/1/012002

Imaging and detection of early stage dental caries with an all-optical photoacoustic microscope

D A Hughes[1], A Sampathkumar[2], C Longbottom[3] and K J Kirk[1]

[1]. School of Physics and Engineering, University of the West of Scotland, Scotland, UK
[2]. F. L. Center for Biomedical Engineering, Riverside Research, New York, USA
[3]. Dental Innovation and Translation Centre, Kings College, London, UK

E-mail: david.hughes@uws.ac.uk

E-mail: ashwin@riversideresearch.org

Abstract. Tooth decay, at its earliest stages, manifests itself as small, white, subsurface lesions in the enamel. Current methods for detection in the dental clinic are visual and tactile investigations, and bite-wing X-ray radiographs. These techniques suffer from poor sensitivity and specificity at the earliest (and reversible) stages of the disease due to the small size (<100μm) of the lesion. A fine-resolution (600 nm) ultra-broadband (200 MHz) all-optical photoacoustic microscopy system was is used to image the early signs of tooth decay. *Ex-vivo* tooth samples exhibiting white spot lesions were scanned and were found to generate a larger (one order of magnitude) photoacoustic (PA) signal in the lesion regions compared to healthy enamel. The high contrast in the PA images potentially allows lesions to be imaged and measured at a much earlier stage than current clinical techniques allow. PA images were cross referenced with histology photographs to validate our experimental results. Our PA system provides a non-contact method for early detection of white-spot lesions with a high detection bandwidth that offers advantages over previously demonstrated ultrasound methods. The technique provides the sensing depth of an ultrasound system, but with the spatial resolution of an optical system.

1. Introduction

Dental caries remains as one of the most common oral diseases in the world [1]. It is the bacterially mediated demineralisation of the hard tissues of the teeth: enamel and dentin [2]. Under normal oral hygienic conditions, the hard tissues of the teeth (enamel and dentin) undergo a constant cycle of demineralisation and re-mineralisation. However, if the environmental pH of the tooth drops below 5.5, demineralization proceeds faster than remineralisation, interrupting the balance of this cycle. Naturally occurring bacteria in the mouth feed on the sugary remnants of food and produce acidic waste products that increase the acidity [2].

At the early stages of the disease, caries manifests as small (<100μm) sub-surface lesions, containing exogenous organic material, appearing as white 'spots' on the tooth surface (as shown in Figure 1). If undiagnosed, the lesion grows in size, spreading through the dentin layer. A cavity occurs when the lesion's surface is disrupted. After this, the process accelerates eventually producing an infection extending to the pulp chamber (which contains nerves and blood vessels) causing inflammation and pain. At this point the tooth would either be extracted, or a filling put in place.

If the caries lesion is detected at a sufficiently early stage, treatment regimes such as increased brushing and flossing or fluoride treatments, can be prescribed which can reinstate the normal mineralisation cycle and thereby halt and possibly reverse the progression of the disease. Current methods for detecting and diagnosing dental caries employing the dental explorer and X-ray radiography are subjective and not quantitative, and therefore are unreliable at the early (reversible) stages of the disease. Furthermore, the dental-explorer technique cannot be guaranteed to be non-invasive, and radiography carries safety risks regarding the use of ionizing radiation. The motivation behind this work is to develop a non-contact, non-invasive and non-ionizing technique to detect early-stage caries and to provide quantitative information for lesion evaluation.

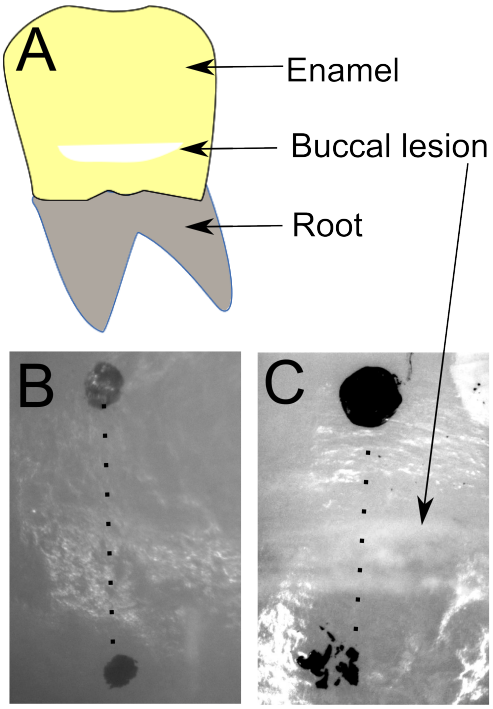

Figure 1. Diagram of a tooth showing a lesion on the buccal surface (A), and photographs of enamel surfaces showing positions of scans over (B) healthy and (C) lesioned areas. Start and end points of the scan are marked with black spots

Several ultrasonic dental imaging methods have been investigated in recent years. These range from conventional pulse-echo imaging at mid-level frequencies [3, 4, 5], CHIRP encoded imaging [6], to laser detected CHIRP encoded imaging [7]. A full review of dental uses of ultrasound is outside the scope of this article, and therefore the reader is directed towards the many comprehensive reviews of the subject [8, 9, 10]. High frequency ultrasound has recently been demonstrated for detecting dental caries [11, 10]. However, the images suffer from poor contrast between healthy and diseased enamel. In addition, conventional ultrasound also requires a coupling medium between the acoustic source and tooth which is impractical in a dental clinic.

Photoacoustic imaging (PA) is emerging as a new modality for non-invasive medical imaging and diagnosis [12, 13, 14, 15]. The PA effect is the generation of ultrasonic waves after absorption of a pulse of light in a material. PA imaging has also been demonstrated with dental tissues [16, 17, 18, 19]. Typically, these studies use a UV light source at a wavelength strongly absorbed [19] by the enamel since these lasers tend to be available to the dental clinician for more

destructive cleaning techniques.

1.1. Theory of detecting tooth decay with PA

In the work presented here, a wavelength of light is chosen that has a stronger absorption coefficient in the caries lesion than the surrounding enamel. A larger PA response is expected from white spot lesions compared to the surrounding healthy enamel due to the higher absorption producing a greater change in temperature. This can be demonstrated by considering the one dimensional temperature distribution for a material exposed to a nanosecond pulse of energy [17]:

$$T(z) = \frac{\mu_a \psi(z)}{\rho C_p} \tag{1}$$

Where $T(z)$ is the temperature at depth z, μ_a is the optical absorption coefficient, $\psi(z)$ is laser energy density (the fluence) at z, ρ is the density of the material, and C_p is the specific heat capacity of the material. The laser energy density can be assumed to follow the Beer Lambert Law, such that

$$\psi(z) = E_0 e^{-\mu_a z} \tag{2}$$

Where E_0 is the energy at the surface of the material and μ_a and z as before. For completeness, the heat equation should be considered to take into account the thermal diffusion during the excitation. However, for nano-second pulses, it is found that the diffusion acts on a much longer time scale and can be neglected.

$$\frac{\partial T}{\partial t} = k_e \bigtriangledown^2 T + h(t) \tag{3}$$

Where T is the temperature, k_e is the thermal diffusivity coefficient, and $h(t)$ is a function describing the input of energy (in this case, laser pulse, $\psi(z)$ convolved with a Gaussian pulse shape). From these equations, it is possible to model the relative PA signals generated from healthy enamel and white spot lesions by incorporating values found in the literature (Shown in table 1). The results of this are shown in figure 2 where the PA signal from a white spot lesion is found to be around double that of a signal excited in healthy enamel. The data shown in Figure 2 is the derivative of the pressure, simulating the output from the interferometer used in the experimental system shown in Figure 2.2. This simplistic treatment only takes absorption into account but it is expected that the higher scattering co-efficient of white spot lesions to enamel will increase the magnitude of the Fluence term ($\phi(z)$) which will also increase the generated photoacoustic signal[17].

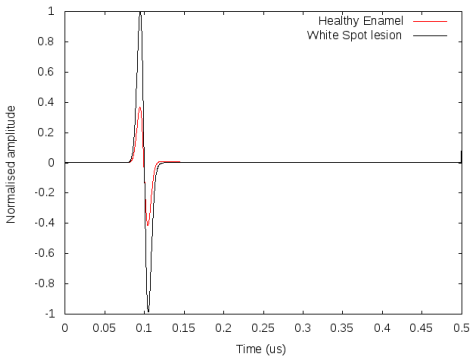

Figure 2. Analytically modelled PA signals excited in healthy enamel and white spot lesions.

Parameter	Healthy enamel	White spot lesion	Ref
μ_a (mm^{-1})	0.02	0.04^a	[20]
ρ (gcm^{-3})	2.65-2.89	1.48-2.0	[21]
C_p $(Jkg^{-1}K^{-1})$	720	945^b	[22]
k_e (m^2s^{-1})	3.22×10^{-7}	3.81×10^{-7}	[23, 24]

[a]Estimated value, [b]calculated from parameters in [22].

Table 1. Optical and thermal parameters of dental tissue.

The PA approach is improved by adopting an all-optical detection technique to eliminate the need for a coupling agent, similar to the work of [18, 19] but with a much greater detection bandwidth to resolve the caries lesions for imaging purposes. This paper describes PA imaging of early-stage caries using an all optical PA microscope. PA signals are generated using a Nd:YAG (Neodymium-doped Yttrium Aluminum Garnet) laser operating at 532 nm with a 5ns pulse duration. The light-induced broadband ultrasound wave is detected at the surface of the tooth with a path-stabilised Michelson interferometer. There are several methods to produce 2D images from PA signals [25, 26, 27]. In this work, the k-wave method is applied using with the K-Wave toolbox[28] in Matlab. The reconstructed PA images of ex-vivo tooth samples containing lesions demonstrate the high sensitivity and feasibility of this technique for detecting and evaluating early stage caries.

2. Materials and Methods

2.1. Sample Preparation

Teeth extracted during orthodontic procedures in a dental clinic were stored in phosphate-buffered saline solution containing thymol to prevent bacterial growth. Samples were visually inspected under bright-field microscopy and regions presenting white spot lesions in the buccal (cheekside) region were identified for scanning under the all-optical PA microscope as shown in Figure 1A. No lapping or polishing was performed on the samples in order to demonstrate the feasibility of the PA microscope in a clinical setting.

The scan area for PA imaging of the tooth was demarcated using a marker pen as shown in Figures 1B and 1C. A linear scan was performed from top to bottom between the marked regions on the tooth. These locations were chosen so that the scan would begin in an area of healthy enamel, travel through the lesion and end in an area of healthy enamel as indicated in Figure 1C. Control samples that showed no signs of disease were imaged similarly using the PA microscope as illustrated in Figure 1B.

2.2. PA Imaging

A schematic diagram of the PA microscope is shown in Figure 2. A frequency-doubled Nd:YAG pulsed laser operating at 532 nm served as a pump source to excite PA effects in tooth. The laser produced 5-ns pulses at 10 Hz with a peak energy of 25 mJ/pulse. The pump light pulses were delivered to the tooth using a liquid-filled light guide in a backward-mode configuration. The sample was mounted on a three-axis, precision stage that allowed 2D scanning of the sample.

The PA-induced surface motion of the sample was detected by a path-stabilized Michelson interferometer [29]. The interferometer used a frequency-doubled Nd:YAG continuous-wave laser with a peak power of 300 mW operating at 532 nm as the detection beam. The output of the laser was collimated and split into a signal beam (i.e. the probe beam) and a reference beam. The probe beam was directed to a mirror and focused to a point on the tooth by the 50X objective. The spot size of the probe beam on the sample surface was measured to be 0.484 μm at the full-width half-maximum point. The probe beam was phase modulated by the motion

of the sample surface and was reflected back to the beam splitter where it interfered with a reference beam that was reflected from a mirror mounted on a piezo-stack. The interfering beams were directed to a high-speed photo-detector with GHz bandwidth. The output of the photo-detector was amplified and directed to an oscilloscope that measured the time-domain signal with respect to a reference trigger derived from the pulsed pump laser.

PA data were collected along a linear scan of 3mm (Figure 1) with a step size of 10 μm. At each scan point, the tooth was moved to the focal plane of the objective to provide maximal detection sensitivity.

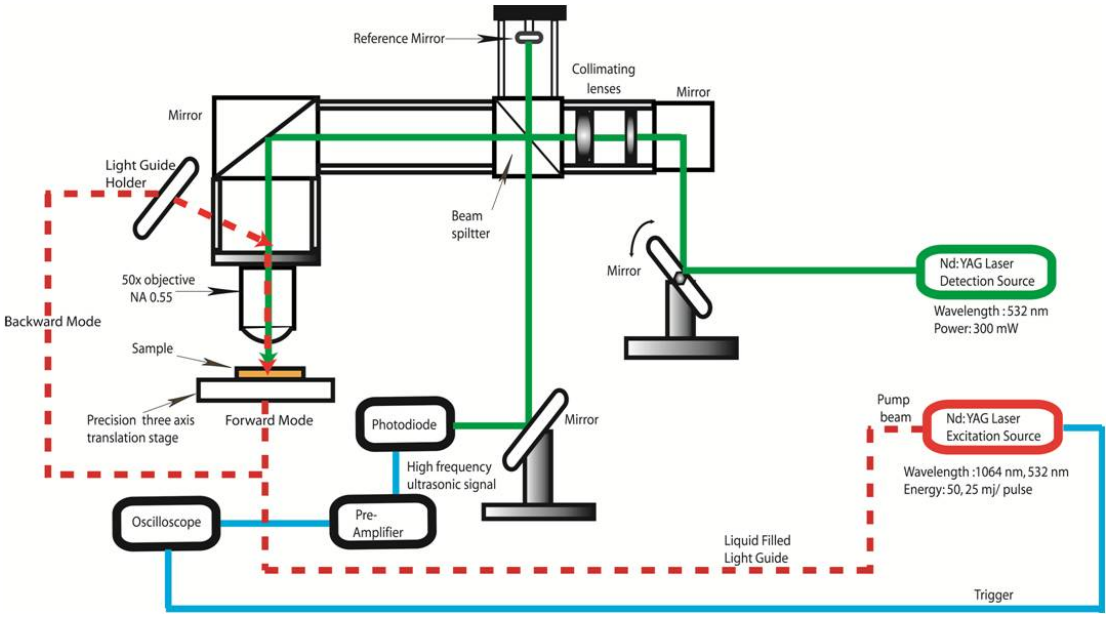

Figure 3. Diagram of all-optical PA microscope system.

2.3. Image Reconstruction

The measured time-domain signal is the superposition of the PA signals originating from all locations within the illuminated region of the tooth that contain light-absorbing chromophores. Materials with a higher optical absorption, such as a lesion, excited at a particular optical wavelength (532 nm) will generate a stronger PA signal. Spatial distributions and relative concentrations of various chromophores can be inferred by employing time-reversal processing of measured time-domain signals[26]. The reconstructed time-domain signals provide the time of arrival of the optically generated acoustic waves over the tooth surface. By knowing the speed of sound in the tooth (a value of $6500ms^{-1}$[30] is used), the acoustic signals can be spatially resolved and back-projected to form a 2D or 3D map of optical-absorption properties. Many sophisticated algorithms, like the inverse spherical-Radon transform or Fourier reconstruction[31], are available to reconstruct the distribution of optical absorbers [25].

In this study, a k-space reconstruction method [26, 32],implemented with the K-wave toolbox in Matlab [28], was used to obtain the absorption properties. This method solves the inverse problem of PA imaging by using back-propagating algorithms to reconstruct the absorbed optical energy distribution from the time-dependent PA signals. In most cases, this distribution depicts the local absorption coefficient at a particular optical wavelength concurrently with the incident light distribution and hence it provides an indirect representation of the optical properties of the tooth. In order to map the true morphology and any potential pathology, quantitative absorption

information, independent of the fluence and wavelength of the light source, is required. The k-space reconstruction algorithm recovers this information by using an iteratively applied forward model of light transport[27]. This algorithm produces a spatial distribution of the absorption coefficient, which is directly related to the spatial distribution of absorbing tissue chromophores and produces quantitative absorption maps that are directly related to specific chromophores.

The PA signal generated at the laser focal point propagates in all directions through the tooth, with reflected ultrasound wavelets arriving at the surface later in time to the initial light pulse. Thus, the displacements measured by the interferometer can also result from ultrasound reflected from an unknown number of reflectors in the tooth.

3. Results

Representative ultrasonic RF-signal data collected from areas of healthy and lesioned enamel are shown in Figure 4A. These are normalised to the white spot lesion signal to emphasise the increased return signal and to allow for easy comparison with the modelled results in figure 2 where a similiar increase of signal is found. These data alone could be used to detect a lesion on the surface of the tooth. However, no quantitative data are provided on the depth to which the lesion has grown and therefore it is useful to reconstruct the PA signal.

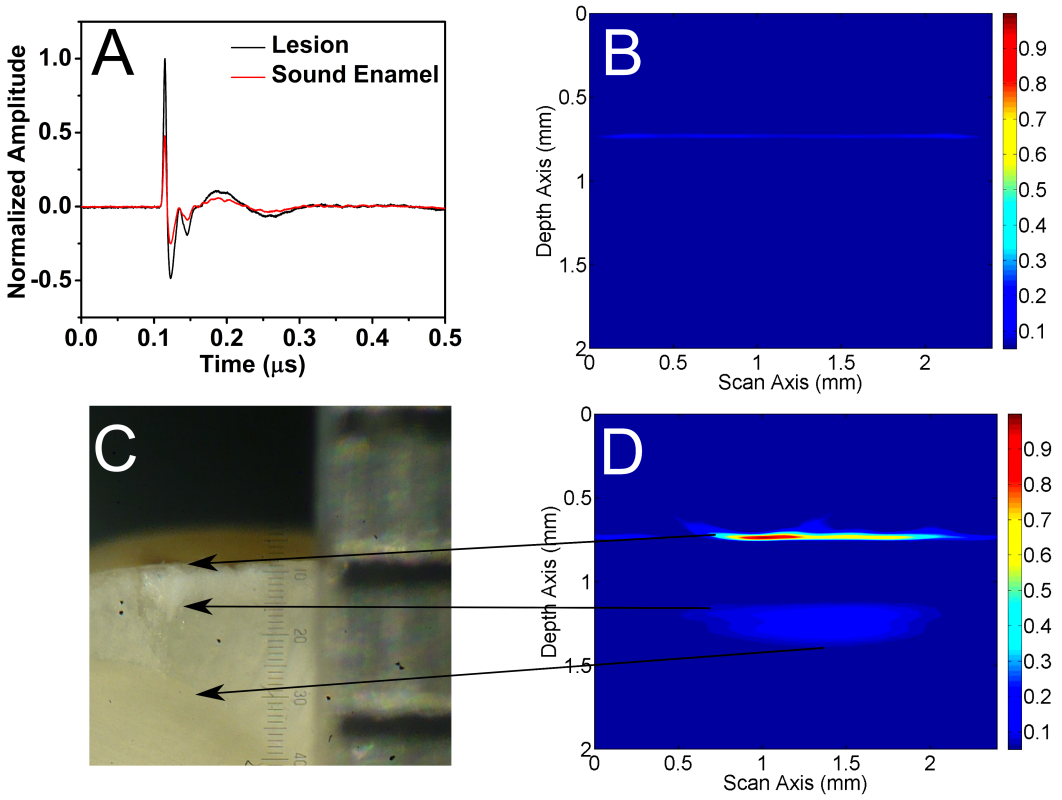

Figure 4. Raw RF-signal data collected from the PA microscope is shown in A, with the reconstructions of healthy enamel and enamel presenting a lesion shown in B and D respectively. A photograph of the hemisected lesion presenting sample is shown in C.

The time-reversal reconstructions of the PA scans are shown in Figure 4B and 4D. Both images have been normalised to the maximal amplitude, and both demonstrate the larger PA signal emerging from the lesion. Figure 4B shows an expanse of blue with a subtle PA signal (not

more than 0.4 in the normalised scale), whereas Figure 4D shows a clear area of increased signal (¿0.6 in the normalised scale) coming from the white spot lesion. The increase of PA signal at the lesion is also apparent in Figure 4D where the signal drops off by an order of magnitude in the healthy enamel either side of the lesion.

We also observed some features beneath the lesion in Figure 4D that do not appear under the healthy enamel. The dimensions of this feature correspond to the geometry of the lesion shown in Figure 4C. The depth of the lesion in the PA image is found to be 0.4 mm, compared to 0.38 mm in the histological image. The thickness of the enamel (measured from the surface to the enamel dentine junction EDJ) was 0.6 mm in the PA image, and 0.84 mm in the histological image. The slight mismatch in the measured dimensions, such as the thickness of the lesion, and the distance to the enamel-dentine junction, is most likely attributed to the defined speed of sound value in the k-wave toolbox ($6500ms^{-1}$). The speed of sound in enamel has been shown to vary with depth, and the lesion itself will exhibit a lower velocity. From the measurements presented here, there is a 3% error in the measurement of the lesion thickness in the image, which corresponds closely to the measurements of changes in velocity of sound due to a white spot lesions [33]. The error in the measurement to the enamel dentine junction is much more pronounced at 30%, and while the velocity will change with depth (due to the structure of the enamel close to the EDJ)[33], further experiments and analysis will have to be carried out to rule out other factors such as the very small amplitude of the propagating ultrasound wavelet, the high attenuation in the dental hard tissues and the viewing aperture of the k-wave algorithm.

The amplitude of the PA signal was maximal at the surface of the tooth where the laser was focused. In order to reconstruct an image of the sub-surface features, the generated ultrasound wave must propagate through the tooth and be reflected from the boundaries between the different materials, e.g. enamel, lesioned enamel and dentine. The key parameter in these reflections is acoustic impedance, with healthy enamel and dentine having values of 16.5MRayls and 8MRayls[34] respectively. Early stage lesions have a slightly lower acoustic impedance than enamel, with the value corresponding to the degree of the disease. Reflected PA waves therefore have a much lower amplitude than generated PA waves, and consequently reflected waves are detected only if they have sufficient amplitude to cause an optical path-length difference in the interferometer.

For imaging, an ideal RF dataset for the time-reversal algorithm would be obtained using a tomographic configuration utilising detectors placed all around the tooth to provide a full viewing aperture. However, in the system presented here, the detection only occurs at the tooth surface and therefore only waves traveling in a specific direction are detected.

4. Conclusions

The all-optical PA microscope appears to be a promising tool for detecting early-stage caries on the surface of teeth. Lesions can be detected because of their larger PA signal amplitudes compared to the PA signal amplitudes generated by healthy enamel. Furthermore, the depth of a lesion can be measured from a time-reversal reconstruction of the RF data. The method has a number of advantages over traditional ultrasound methods such as improved contrast between lesioned and healthy enamel and no requirement for a coupling medium between the source and the tooth. These studies are now continuing with emphasis on miniaturising the system and improving our understanding of the k-wave algorithms for our application's data.

References

[1] Bagramian R A, Garcia-Godoy F and Volpe A R 2009 *American journal of dentistry* **22** 3–8 ISSN 0894-8275
[2] Selwitz R H, Ismail A I and Pitts N B 2007 *Lancet* **369** 51–9 ISSN 1474-547X URL http://www.ncbi.nlm.nih.gov/pubmed/17208642
[3] Ślak B, Ambroziak A, Strumban E and Maev R G 2011 *Acta of bioengineering and*

biomechanics / Wrocaw University of Technology **13** 65–70 ISSN 1509-409X URL http://www.ncbi.nlm.nih.gov/pubmed/21500765

[4] Hughes D A, Girkin J M, Poland S, Longbottom C, Button T W, Elgoyhen J, Hughes H, Meggs C and Cochran S 2009 *Ultrasonics* **49** 212–8 ISSN 1874-9968 URL http://dx.doi.org/10.1016/j.ultras.2008.08.007

[5] Culjat M, Singh R S, Yoon D C and Brown E R 2003 *IEEE transactions on medical imaging* **22** 526–9 ISSN 0278-0062 URL http://ieeexplore.ieee.org/articleDetails.jsp?arnumber=1200928

[6] Harput S, Evans T, Bubb N and Freear S 2011 *IEEE transactions on ultrasonics, ferroelectrics, and frequency control* **58** 2096–106 ISSN 1525-8955 URL http://ieeexplore.ieee.org/xpls/abs_all.jsp?arnumber=6039999' escapeXml='false'/>

[7] Santos S D, Domenjoud M and Prevorovsky Z 2010 *Physics Procedia* **3** 913–918 ISSN 18753892 URL http://dx.doi.org/10.1016/j.phpro.2010.01.117

[8] Ghorayeb S R, Bertoncini C A and Hinders M K 2008 *IEEE transactions on ultrasonics, ferroelectrics, and frequency control* **55** 1256–66 ISSN 1525-8955 URL http://www.ncbi.nlm.nih.gov/pubmed/18599413

[9] Xiang X, Sowa M G, Iacopino A M, Maev R G, Hewko M D, Man A and Liu K Z 2010 *Journal of periodontology* **81** 186–98 ISSN 1943-3670 URL http://www.ncbi.nlm.nih.gov/pubmed/20151796

[10] Marotti J, Heger S, Tinschert J, Tortamano P, Chuembou F, Radermacher K and Wolfart S 2013 *Oral surgery, oral medicine, oral pathology and oral radiology* **115** 819–832 ISSN 2212-4411 URL http://www.ncbi.nlm.nih.gov/pubmed/23706922 http://www.sciencedirect.com/science/article/pii/S2212440313001727

[11] Hughes D A, Girkin J M, Poland S, Longbottom C and Cochran S 2009 *2009 IEEE International Ultrasonics Symposium* (IEEE) pp 1–3 ISBN 978-1-4244-4389-5 URL http://ieeexplore.ieee.org/xpls/abs_all.jsp?arnumber=5441480 http://ieeexplore.ieee.org/lpdocs/epic03/wrapper.htm?arnumber=5441480

[12] Kruger R A, Liu P, Fang Y R and Appledorn C R 1995 *Medical physics* **22** 1605–9 ISSN 0094-2405 URL http://www.ncbi.nlm.nih.gov/pubmed/8551984

[13] Oraevsky A A, Jacques S L, Esenaliev R O and Tittel F K 1994 *Society of Photo-Optical Instrumentation Engineers (SPIE) Conference Series* **2134** 122 ISSN 0277-786X URL http://adsabs.harvard.edu/abs/1994SPIE.2134A.122O

[14] Zhang H F, Maslov K, Stoica G and Wang L V 2006 *Nature biotechnology* **24** 848–51 ISSN 1087-0156 URL http://www.ncbi.nlm.nih.gov/pubmed/16823374

[15] Zhang E, Laufer J and Beard P 2008 *Applied Optics* **47** 561 ISSN 0003-6935 URL http://ao.osa.org/abstract.cfm?URI=ao-47-4-561

[16] Wang H c, Fleming S, Lee Y c, Swain M and Law S 2011 *Biomedical optics express* **17** 345–355

[17] Li T and Dewhurst R J 2010 *Journal of Physics: Conference Series* **214** 012028 ISSN 1742-6596 URL http://iopscience.iop.org/1742-6596/214/1/012028

[18] Wang H c, Fleming S, Lee Y c, Law S and Swain M 2009 *Optics express* **17** 157–163

[19] Blodgett D W 2003 *The Journal of the Acoustical Society of America* **114** 542 ISSN 00014966 URL http://scitation.aip.org/content/asa/journal/jasa/114/1/10.1121/1.1578080

[20] Spitzer D and Bosch J T 1975 *Calcified tissue research* **17** 129–37 ISSN 0008-0594 URL http://www.ncbi.nlm.nih.gov/pubmed/1139366

[21] Huang T T Y, Jones A S, He L H, Darendeliler M A and Swain M V 2007 *Journal of dentistry* **35** 737–43 ISSN 0300-5712 URL http://www.sciencedirect.com/science/article/pii/S0300571207001133

[22] Hellen A 2010 *Quantitative Evaluation of Simulated Enamel Demineralization and Remineralization Using Photothermal Radiometry and Modulated* Ph.D. thesis University of Toronto

[23] Minesaki Y 1990 *Shika zairy, kikai = Journal of the Japanese Society for Dental Materials and Devices* **9** 633–46 ISSN 0286-5858 URL http://www.ncbi.nlm.nih.gov/pubmed/2134829

[24] Xu H C, Liu W Y and Wang T 1989 *Australian dental journal* **34** 530–5 ISSN 0045-0421 URL http://www.ncbi.nlm.nih.gov/pubmed/2619623

[25] Xu M and Wang L 2005 *Physical Review E* **71** 016706 ISSN 1539-3755 URL http://link.aps.org/doi/10.1103/PhysRevE.71.016706

[26] Cox B T and Beard P C 2005 *The Journal of the Acoustical Society of America* **117** 3616 ISSN 00014966 URL http://scitation.aip.org/content/asa/journal/jasa/117/6/10.1121/1.1920227

[27] Cox B T and Arridge S R 2005 *SPIE BIOS* January pp 49–55

[28] Treeby B E and Cox B T 2010 *Journal of biomedical optics* **15** 021314 ISSN 1560-2281 URL http://biomedicaloptics.spiedigitallibrary.org/article.aspx?articleid=1103324

[29] Sampathkumar A, Chitnis P V and Silverman R H 2014 *SPIE BiOS* ed Oraevsky A A and Wang L V (International Society for Optics and Photonics) p 89432Y URL http://proceedings.spiedigitallibrary.org/proceeding.aspx?articleid=1840446

[30] Huysmans M C and Thijssen J M 2000 *Journal of dentistry* **28** 187–91 ISSN 0300-5712 URL http://www.ncbi.nlm.nih.gov/pubmed/10709340
[31] Jaeger M, Schüpbach S, Gertsch A, Kitz M and Frenz M 2007 *Inverse Problems* **23** S51–S63 ISSN 0266-5611 URL http://stacks.iop.org/0266-5611/23/i=6/a=S05
[32] Cox B T, Kara S, Arridge S R and Beard P C 2007 *The Journal of the Acoustical Society of America* **121** 3453–64 ISSN 1520-8524 URL http://www.ncbi.nlm.nih.gov/pubmed/17552697
[33] Maev R G, Denisova L A, Maeva E Y and Enissov A A 2002 *Ultrasound in medicine & biology* **28** 131–136
[34] Culjat M O, Goldenberg D, Tewari P and Singh R S 2010 *Ultrasound in medicine & biology* **36** 861–73 ISSN 1879-291X URL http://www.sciencedirect.com/science/article/pii/S030156291000075X